Proceedings of the 11th ICPMG 2026
11th International Conference on Physical Modelling in Geotechnics
8-12 June 2026, Zurich, Switzerland

Physical and numerical modeling of cone penetration to support critical state line-based CPTu interpretation

S.A. Beltran
Portland State University, Portland, USA, sbeltran@pdx.edu
B. K. Auyeung
Portland State University, Portland, USA, bauyeung@pdx.edu
D.M. Moug
Portland State University, Portland, USA, dmoug@pdx.edu

ABSTRACT: Current cone penetration test (CPTu) interpretation methods rely heavily on empirical correlations to estimate soil parameters such as relative density, over-consolidation ratio, and initial state. While effective for "standard soils" such as quartz and silica-based sands, these correlations tend to be less reliable when applied to "non-standard soils" that fall outside the range of the datasets used to develop the correlations. This study leverages centrifuge modeling to support numerical modeling and explore how CPTu measurements relate to fundamental soil behavior. Using centrifuge modeling, CPTu tests were performed in Ottawa F-65 sand to examine cone tip resistance (q_t), normalized tip resistance (q_{t1N}), and sleeve friction (f_s) for relative density of 40% and 80%. Direct penetration numerical modeling of these centrifuge tests is used to simulate the soil's stress path from its initial state to the cone tip and friction sleeve in relation to the soil's critical state line. This supports development of a CSL-based interpretation for CPTu data and provides a first step towards its application to non-standard soils in future work.

1 INTRODUCTION

Current cone penetration test (CPTu) interpretation methods largely rely on empirical correlations from large databases of lab and field test results (e.g. Robertson 2009). Most of these databases are dominated by "standard soils" such as quartz sands and normal clays, so the correlations do not always capture the behavior of "non-standard soils" like calcareous sands or mine tailings. Theory-based approaches to CPTu data interpretation provide an interpretation basis beyond the empirical datasets. However, many of these theory-based approaches assume either normal clay behavior (Chen & Mayne, 1996) or behaviors consistent with quartz sand (e.g., Been & Jefferies, 1985). Expanding theory-based CPT interpretation methods has potential to encompass a range of soil types and behaviors. One such approach is based on the soil's critical state line (CSL). Several previous numerical studies have shown a relationship between cone penetration data and a soil's CSL, including Moug et al. (2019) and Hyder & Moug (2024) that examined the cone tip resistance for silica and calcareous sands in relation to the position of each soil's CSL and the initial state.

This study supports a CSL-based approach to interpret CPTu data. Figure 1 schematically illustrates how a soil element moves through different stress states relative to the CSL during cone penetration. The soil is initially at static in-situ conditions at point O. As the soil is loaded by the cone, the soil is loaded to point A on the CSL just ahead of the cone tip. From the cone tip to the cone shoulder (point B), soil loading conditions are along the CSL, suggesting that the cone tip resistance relates to the stress conditions along the CSL. Finally, soil is unloaded as it transitions from the cone tip to the shaft friction sleeve from points C to D, but the loading conditions appear to be related to the CSL. Mapping these stress paths relative to the CSL suggests that the CSL may provide a consistent, theory-based framework for interpreting CPTu data. Furthermore, since a CSL can be defined for standard and non-standard soils, this approach can be explored as a CPTu interpretation method that can be applied to many soil types.

Development of a CSL-based CPTu interpretation framework requires CPTu measurements including cone tip resistance (q_t), sleeve friction (f_s), and shoulder porewater pressure (u_2) for soil profiles with known soil types, conditions, and initial state. Physical modeling is used in this study to collect CPTu data from a uniform soil profile with controlled initial conditions. Additionally, numerical modeling of direct cone penetration is used to examine the loading path relative to the CSL during cone penetration. q_t and f_s

measurements are collected from 10 mm diameter cone profiles in a centrifuge model of Ottawa F-65 sand. The model was prepared with sand at 41% and 81% relative density (D_r). Cone penetration is numerically simulated through an axisymmetric direct penetration model to yield simulated q_t and f_s values. The physical model results are used to validate numerical simulations. The simulated soil loading path relative to the CSL during cone penetration is examined.

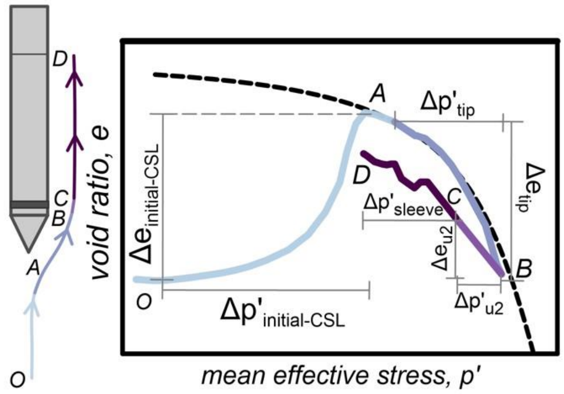

Figure 1. Schematic of loading path to CSL with CPTu.

2 CENTRIFUGE MODEL

Centrifuge tests were carried out at the Natural Hazards Engineering Research Infrastructure (NHERI) Center for Geotechnical Modeling (CGM) at the University of California, Davis during the summer of 2025. The UC Davis centrifuge has a 9 meter radius and operates by spinning a scale model mounted at the end of its arm. As the arm rotates, the increased centripetal acceleration raises the gravitational field acting on the model. This allows prototype-level stresses to be recreated in a reduced-scale configuration.

2.1 Container and cone profiles

A custom model container was built to collect CPTu data while minimizing container boundary effects. The setup allowed multiple CPTu pushes to be performed on loose and dense sand across different stress conditions in a single spin model.

The soil model was composed of two circular chambers, one to contain loose soil and the other dense soil, positioned side by side and spaced approximately 280 mm from each other, as shown in Figure 2. Both chambers were fabricated from 6.3 mm thick steel sheets that were laser-cut and rolled to form two cylinders, each 660 mm in diameter. The inner halves of the chambers, which face each other, were 508 mm tall, while the outer halves extended to a height of 635 mm. These taller outer halves form a continuous wall that spans across the central gap between the chambers, thereby creating a shared region between them that is used as a water reservoir. The reduced height of the inner walls allows a uniform water level to be maintained across both soil chambers. The entire assembly was mounted on a 9.5 mm thick steel base plate.

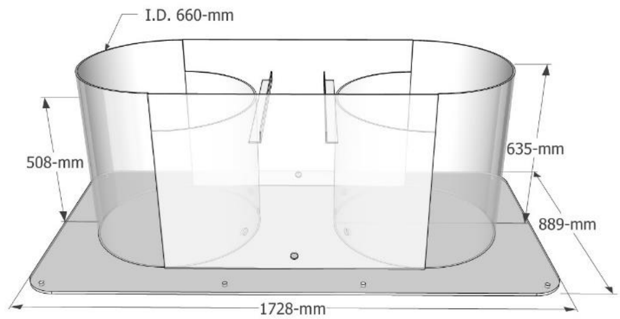

Figure 2. Rendering of centrifuge model container.

Model boundary conditions were consistent with recommended ratios. Bolton et al. (1997) suggest that the container diameter (D) to cone diameter (B) ratio (D/B) should be at least 30; both chambers satisfy this criterion with D/B = 66. The distance from a cone push to the nearest wall (S) to B ratio (S/B) should be at least 10. For the 10 mm cones used, S/B ranged from 10.5 to 34.5; for the 6 mm cone used, S/B ranged from 10.5 to 14.

The "zone of influence" is the region of soil affected by penetration and it typically extends 10B to 20B from the penetrating cone (Lunne et al., 1997). To avoid interaction between cone profiles, overlap of the zones of influence was minimized, but could not be eliminated for all profiles. The cone profile spacings were 11B to 18B for the 10 mm cones and 13.5 to 18.5 cone diameters for the 6 mm cone, as shown in Figure 3.

2.2 Soil

Ottawa F-65 sand was selected as the baseline soil for this study so that results could be compared directly with previous work, and because very little centrifuge data exists for this sand that includes f_s measurements. Models were prepared with dry pluviation to Dr of 41% and 81% for a "loose" and "dense" preparation, respectively. Index properties for Ottawa F-65 sand were consistent with those characterized in the LEAP-UCD-2017 program. The minimum and maximum densities are 1457 kg/m^3 and 1754 kg/m^3, respectively, with corresponding minimum and maximum void ratios of 0.51 and 0.78. The specific gravity is 2.65.

2.3 Saturation

The models were saturated with bottom-up flooding with tap water during spinning at 20g. In-flight flooding at 20g allowed fast saturation while reducing the likelihood of trapped air because the height of capillary rise is inversely related to the model g-level (Kutter, 2012). The expected degree of saturation at 20g is about 95%, based on the Bond and Capillary Number framework from Kutter (2012). This was considered a sufficiently high degree of saturation for u_2 measurements in sand, which were expected to measure static porewater pressures. Additionally, the centrifuge requires counterweights on the centrifuge arm to offset the model weight (including soil and water). It was likely that adding too much water at higher g-levels would unbalance the spinning centrifuge arm.

In-flight model flooding was carried out using two vertical standpipes located within the central water reservoir, with one standpipe positioned adjacent to each soil chamber. Each standpipe was 25.4 mm in diameter and 470 mm tall, with its top located approximately 30 mm below the soil surface. Each soil chamber was fitted with three water inlets along its base on the side facing the reservoir, and each standpipe was connected to its corresponding chamber through three hoses, linking the standpipe outlets to the chamber base inlets. A plan view of the model with the standpipes, connections, and drains is shown in Figure 3.

Stage 1 of flooding was performed prior to spinning, during which the central reservoir was filled to a height of 381 mm (approximately 106 L) with water, which was below the standpipe overflow level. Stage 2 of flooding was initiated in-flight at 20g, at which point additional water was introduced into the reservoir. Water entered the standpipes from the top and flowed into the soil chambers through the base inlets. The water level rose within both chambers and eventually reached equilibrium at a height of approximately 560 mm, corresponding to 60 mm above the soil surface. Approximately 216 L of water was added during this second stage. After flooding, the centrifuge was spun down for rebalancing through application of counterweights.

2.4 Cone penetrometer and sensors

Three cone penetrometers were used in this model: a 6 mm LEAP CPT, a 10 mm LEAP CPT, and a 10 mm CPTu. The 6 mm and 10 mm LEAP cones (LEAP-UCD-2017) were fabricated at the CGM following LEAP specifications, while the 10 mm CPTu was purchased from the University of Western Australia.

The 6 mm LEAP cone has a maximum tip capacity of 78.7 MPa and a rod length of 500 mm. The 10 mm LEAP cone has a maximum tip capacity of 56.6 MPa and the same rod length of 500 mm. The 10 mm CPTu includes load cells for q_c and f_s, and a pore pressure transducer at the cone shoulder for u_2 measurements. The maximum capacities for the CPTu are 19.1 MPa for cone tip resistance and 1 MPa for sleeve friction and pore pressure, with a total rod length of 420 mm.

Baseline pore pressure transducers installed at the bottom of each container confirmed hydrostatic conditions prior to cone penetration. Measured pore pressures were consistent with prototype scaling at each g-level, indicating full saturation and absence of residual excess pore pressures following reconsolidation.

CPTu penetration was performed at a rate of 4 mm/s. This penetration rate was expected to be consistent with drained penetration conditions for Ottawa F-65 sand. During penetration with the 10 mm CPTu, the shoulder pore pressure (u_2) reading was consistent with static porewater pressure values, as expected from drained penetration.

Table 1. Summary of CPT/CPTu tests performed

Cone	Condition	OCR
10 mm CPTu	loose 15g	1
10 mm CPTu	dense 15g	1
10 mm CPTu	loose 30g	1
10 mm CPTu	dense 30g	1
10 mm CPTu	loose 48.9g	1
10 mm CPTu	loose 24.5g	2
10 mm CPTu	dense 24.5g	2
10 mm CPTu	loose 12.2g	4
10 mm CPTu	dense 12.2g	4
6 mm CPT	loose 60g	1
6 mm CPT	dense 60g	1
6 mm CPT	loose 30g	2
6 mm CPT	dense 30g	2
10 mm CPT	loose 60g	1
10 mm CPT	dense 60g	1

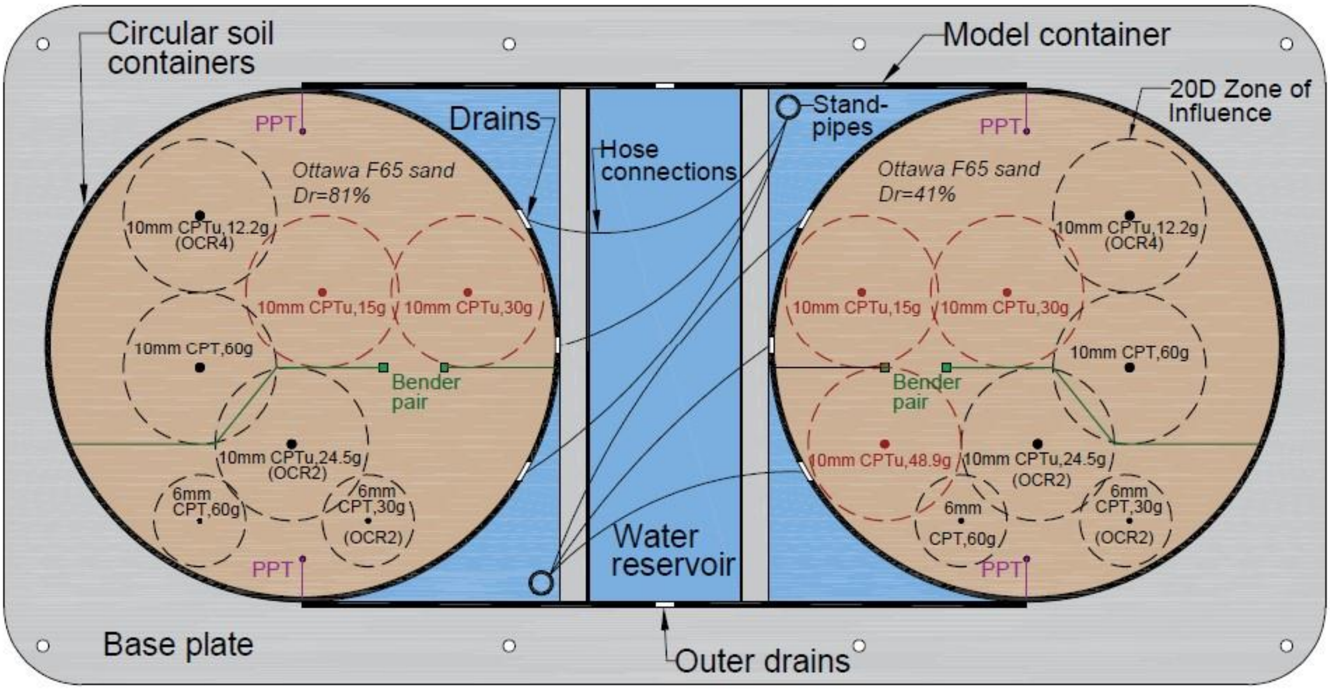

Figure 3. Top view of model with test locations.

Table 1 summarizes the profiles measured for each cone, including soil relative density, g-level, and over consolidation ratio (OCR). Figure 3 shows the location of all cone penetration tests in the Ottawa F-65 sand model. Only the results of OCR = 1, 10 mm CPTu pushes are presented herein and include one loose and one dense test at 15g, one loose and one dense test at 30g, and one loose test at 48.9g.

OCR values reported in Table 1 are defined relative to the maximum g-level reached within each spin. The standard approach used at the CGM is that when the model returns to 1g, stress relaxation resets the stress history. Therefore, the model is considered normally consolidated at the start of each spin. The OCR = 1 results correspond to penetrations performed at the maximum g-level within each stage.

To measure soil stiffness, bender pairs were installed in both the loose and dense chambers at depths corresponding to initial vertical effective stresses of 50, 100, and 200 kPa at 60g. Each pair was calibrated before testing, with sensor spacing between 5 and 7 mm.

Two pore pressure transducers (PPTs) were placed at the bottom of each chamber to verify porewater pressures during flight. Each PPT was calibrated to 345 kPa.

3 NUMERICAL MODEL

Direct cone penetration in Ottawa sand was simulated with an axisymmetric model in FLAC 8.0 (Itasca). Large soil deformations around the penetrating cone are accommodated with a user-defined Arbitrary Lagrangian Eulerian rezoning and remapping scheme, as described in Moug et al. (2019a). Soil was modelled with the MIT-S1 constitutive model (Pestana and Whittle 1999). The MIT-S1 constitutive model was considered advantageous for this study because it can span model behavior from normal clays to sands (Pestana et al. 2002, Pestana and Whittle 2002). The MIT-S1 calibration for Ottawa sand used; this calibration is presented in Moug et al. (2019b) as Calibration 3.

The numerical cone penetration model and boundary conditions are shown in Figure 4. Cone penetration is simulated for a single depth and initial condition in the model profile. Initially the cone is wished into place, then soil is simulated as flowing up past the static cone until steady state conditions are achieved. Rezoning and remapping are regularly performed during simulated penetration to prevent numerical instability and severe zone distortion. Simulated q_t and f_s were found at steady state after 25B of simulated penetration.

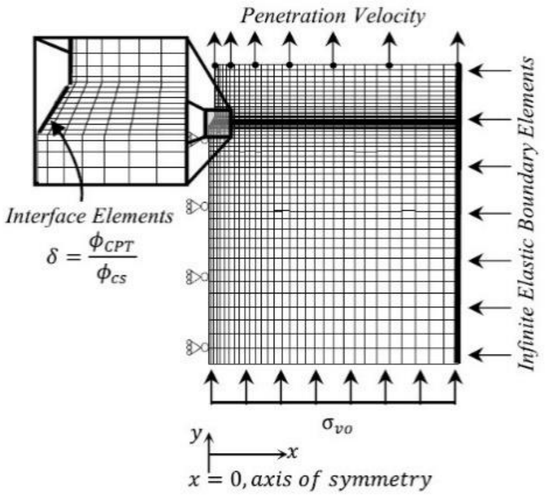

Figure 4. Schematic of CPTu push in FLAC (from Moug et al. 2019a).

The interface between the cone and soil is captured with interface elements of normal and shear springs and is governed by a Mohr-Coulomb friction condition. The friction angle is represented by δ, which is the ratio of the interface friction angle to the soil critical state friction angle. Typical δ values are 0.40 to 0.80 and depend on cone condition (Uesugi and Kishida 1986). Past cone penetration simulations in Ottawa sand used δ = 0.60 (Moug et al 2019b). However, for this study, δ = 0.10 was found to reasonably capture the centrifuge model data. δ = 0.60 resulted in f_s values up to eight times larger and q_t values up to 1.5 times larger than the values measured with the centrifuge models. Other studies have found lower δ values result in reasonable simulated cone penetration data, for example Ahmadi & Golestani Dariani (2017) used an equivalent δ of about 0.17.

Lower-than-typical δ values for these tests may be attributed to the surface condition for the CPTu. It is possible that after further testing, the δ will increase due to wear on the cone. Alternatively, it is possible that the model calibration for Ottawa Sand should be revised to capture soil loading around the cone that results in q_t and f_s. It is expected that the calibration will be revised as additional testing (i.e., triaxial testing to directly characterize the CSL) is performed.

4 RESULTS FROM PHYSICAL AND NUMERICAL CONE PENETRATION MODELS

The results for the 10 mm CPTu cone are presented to examine q_t and f_s measurements. The q_t profiles from the LEAP cones and other OCR values will be presented and analyzed in future publications. Figure 5 shows q_t, q_{t1N}, and f_s versus initial vertical effective stress (σ'_{vo}) at 15g, 30g, and 48.9g for loose (Dr=41%) and dense (Dr=81%) conditions. Profiles for Dr = 81% at 30g and 48.9g did not extend the whole soil profile length due to CPTu capacity limitations. q_{t1N} was estimated with the following equation:

$$q_{t1N} = \left(\frac{q_t}{P_a}\right)\left(\frac{P_a}{\sigma'_{v0}}\right)^m \quad (1)$$

Where P_a is atmospheric pressure and σ'_{v0} is evaluated at the depth corresponding to each q_t measurement. A value of m = 1 was adopted, consistent with centrifuge profiles measured in Sawyer (2018). Although q_{t1N} normalizes well with the above expression for Dr = 41%, the profile for Dr = 81% shows an increasing trend with depth. This trend with depth may be due to effects near the model top

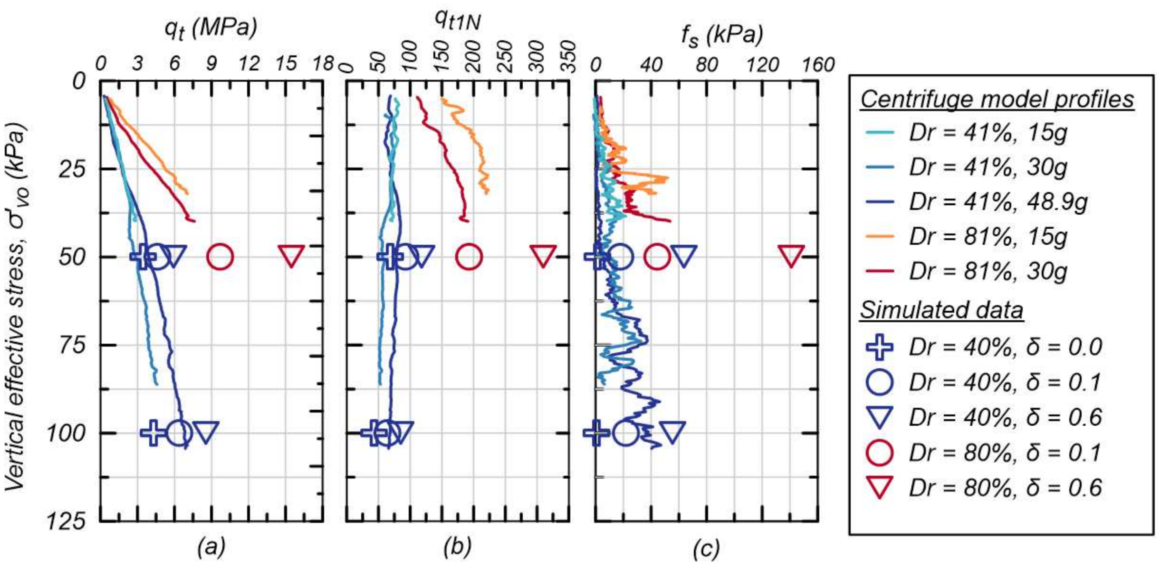

Figure 5. CPTu profiles measured in the centrifuge model compared with simulated CPTu data.

boundary or may indicate that a different m value is appropriate. Additional normalization relationships will be explored for these profiles and accounting for the results with the LEAP cones in future work.

As expected, the q_t, q_{t1N}, and f_s profiles for Dr = 41% are consistently lower than those for Dr = 81% throughout the measured σ'_{v0} profiles. Additionally, q_t and f_s increase with σ'_{v0}. There is some variability of measurements in the f_s profiles, however, the measurements are generally repeatable between the profiles and g-levels.

Simulated values for q_t and f_s, and calculated values of q_{t1N} are also plotted in the profiles of Figure 5 for Dr = 41% with δ = 0, 0.1 and 0.6, and 81% with δ = 0.1 and 0.6. The results show the sensitivity of the simulated data to δ, where q_t and f_s increase as δ increases. As stated above, δ = 0.10 was found to provide reasonable agreement between simulated and measured q_t and f_s values. Comparison of the numerical and physical model results indicate that both q_t and f_s values can be reasonably estimated through the direct penetration model with the Moug et al. (2019) MIT-S1 calibration cone penetration in Ottawa sand.

A possible framework for interpreting CPTu data is based on soil loading relative to the CSL during cone penetration. Figure 6 shows simulated loading paths for loose and dense Ottawa sand in void ratio – mean effective stress (e – p') space for Figure 6a,c and deviatoric stress (q) – p' space for Figures 6b,d. Figures 6a and 6b show the loading from σ'_{v0} = 50 kPa, past the cone tip and to the cone shoulder. Figures 6c and 6d show the loading from the cone shoulder and along the friction sleeve. The loading path from in situ conditions to the cone shoulder, then from the cone shoulder along the friction sleeve are presented separately to limit crowding.

From in situ conditions, the simulated loading paths for both the loose and the dense soil are loaded to the CSL in e - p' space (Figures 6a) ahead of the cone tip. As expected, the dense soil loads to higher stress conditions along the CSL at the cone tip compared to the loose soil, resulting in a higher q_t value. In q - p' space (Figure 6b), loading at a critical state stress ratio develops well ahead of the cone tip although the soil is not at critical state conditions, as shown in Figure 6a. Soil is unloaded as it transitions from the cone tip to the cone shoulder along the CSL, then leaves the CSL in e – p' space by the friction

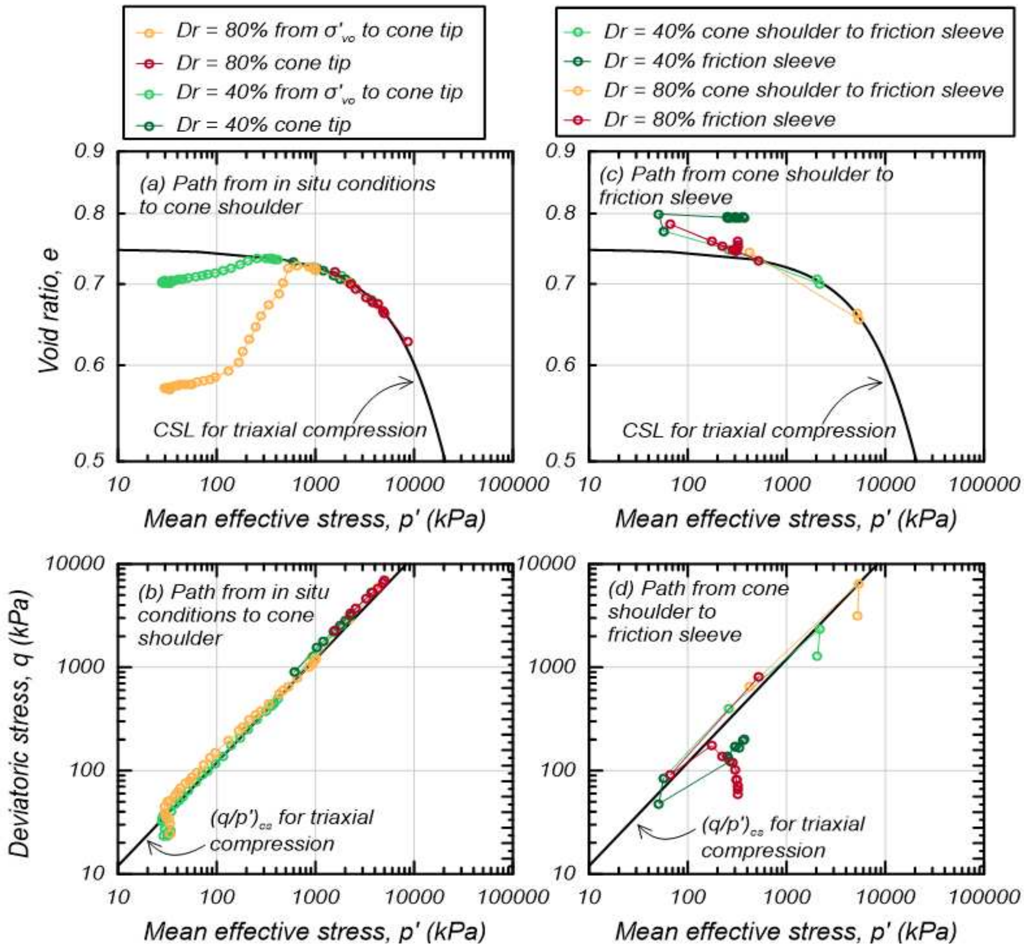

Figure 6. Simulated soil loading paths during cone penetration for Dr = 40% and 80% from σ'_{vo} = 50 kPa

sleeve, as shown in Figure 6c. Loading to the friction sleeve in Figure 6d indicates that unloading takes place along the critical state stress ratio, but unloads below critical state stress ratios by the friction sleeve. For both loose and dense soils, loading is at a nearly steady-state condition for most of the friction sleeve.

5 DISCUSSION

The physical model provided valuable CPTu data for calibration and validation of numerical models. In particular, f_s values had not been previously measured in Ottawa F-65 sand, to the extent of the authors' knowledge. Additional work for this research will include additional numerical analysis for the range of stresses tested in the physical model, and high stress triaxial compression tests to evaluate the calibrated CSL. The numerical modeling and analysis will be expanded, with additional physical modeling and laboratory testing, to develop a theory-based CPTu interpretation approach.

6 CONCLUSIONS

Physical geotechnical centrifuge modeling of CPTu was carried out for loose (Dr = 41%) and dense (Dr = 81%) Ottawa F-65 sand. Cone profiles measured q_t and f_s while u_2 measurements reflected static porewater conditions. A custom designed and built, dual chamber model container was used to allow in-flight water flooding for soil saturation and perform cone penetration profiles in two different soil preparations. CPTu profiles were measured at 15g, 30g, and 48.9g.

Direct cone penetration simulations were performed to simulate q_t and f_s data collected from the physical models. The simulated values reasonably agree with the physical model data when low interface friction conditions are imposed, confirming that q_t and f_s are reasonably captured with the numerical models. This provides a basis for examination of the soil paths during cone penetration and how they relate to the CSL and other fundamental properties for theory-based CPTu interpretation.

ACKNOWLEDGEMENTS

This material is based upon work supported by the National Science Foundation under CAREER Award No. CMMI-2340596. Any opinions, findings, and conclusions or recommendations expressed in this material are those of the authors and do not necessarily reflect the views of the National Science Foundation. The authors also appreciate the support of the faculty, staff, and students at the NHERI Center for Geotechnical Modeling for training, mentoring, and project support.

REFERENCES

Been, K. and Jefferies, M.G. (1985). A state parameter for sands. *Géotechnique*, 35(2), 99–112. http://doi.org/10.1680/geot.1985.35.2.99

Bolton, M.D., Gui, M.W., Garnier, J., Corte, J.F., Bagge, G., Laue, J. and Renzi, R. (1999). Centrifuge cone penetration tests in sand. *Géotechnique*, 49(4), 543–552. http://doi.org/10.1680/geot.1999.49.4.543

Boulanger, R.W. and Idriss, I.M. (2014). *CPT and SPT based liquefaction triggering procedures*. Report No. UCD/CGM-14/01, Center for Geotechnical Modeling, University of California, Davis.

Chen, B.S.-Y. and Mayne, P.W. (1996). Profiling the overconsolidation ratio of clays by piezocone tests. *Canadian Geotechnical Journal*, 33(1), 150–159.

Choo, Y.W., Kim, J.H., Kim, D.J. and Kim, D.S. (2015). Miniature cone tip resistance on sand in a centrifuge. *Journal of Geotechnical and Geoenvironmental Engineering*, 142(3), 04015090. http://doi.org/10.1061/(ASCE)GT.1943-5606.0001425

Giretti, D., Been, K., Fioravante, V. and Dickenson, S. (2017). CPT calibration and analysis for a carbonate sand. *Géotechnique*, 67(11), 955–970. http://doi.org/10.1680/jgeot.16.P.312

Giretti, D., Fioravante, V., Been, K. and Dickenson, S. (2017). Mechanical properties of a carbonate sand from a dredged hydraulic fill. *Géotechnique*, 67(11), 971–988. http://doi.org/10.1680/jgeot.16.P.304

Hibbeler, R.C. (2017). *Mechanics of materials*, 10th ed. Pearson Education, Boston, MA.

Hyder, J. and Moug, D. (2024). Critical state line-based CPTu interpretation using numerical cone penetration modeling. *Proceedings of the International Conference on Physical Modelling in Geotechnics (ICPMG 2024)*.

ISO (2012). *ISO 22476-1: Geotechnical investigation and testing — Field testing — Part 1: Cone penetration test (CPT).* International Organization for Standardization, Geneva, Switzerland.

Jaeger, R.A. (2012). *Numerical modeling of cone penetration in granular materials*. PhD thesis, University of California, Davis.

Kutter, B.L. (2012). Effects of capillary number, Bond number, and gas solubility on water saturation of sand specimens. *Journal of Geotechnical and Geoenvironmental Engineering*, 138(6), 768–780.

LEAP-2017 Committee (2017). *Liquefaction Experiments and Analysis Projects (LEAP): Summary and guidance*. ISSMGE Technical Committee TC104.

Meng, J., Boulanger, R.W. and DeJong, J.T. (2006). Observations from in situ testing within a calcareous soil. *Journal of Geotechnical and Geoenvironmental Engineering*, 132(6), 779–791.

Moug, D. and Price, A.B. (2023). Examination of cone penetration in non-plastic silt with a direct cone penetration model. *Journal of Geotechnical and Geoenvironmental Engineering*, 149(2), 04022159.

Moug, D. M., Price, A. B., Parra Bastidas, A. M., Darby, K. M., Boulanger, R. W., & DeJong, J. T. (2019). Mechanistic development of CPT-based cyclic strength correlations for clean sand. *Journal of Geotechnical and Geoenvironmental Engineering*, *145*(10), 04019072.

Moug, D., DeJong, J.T. and Boulanger, R.W. (2019). Axisymmetric simulations of cone penetration in saturated clay. *Journal of Geotechnical and Geoenvironmental Engineering*, 145(3), 04018105.

Moug, D., DeJong, J.T. and Boulanger, R.W. (2019). Mechanistic development of CRR–qc relationships. *Journal of Geotechnical and Geoenvironmental Engineering*, 145(8), 04019045.

Moug, D. M., Boulanger, R. W., DeJong, J. T., & Jaeger, R. A. (2019). Axisymmetric simulations of cone penetration in saturated clay. *Journal of Geotechnical and Geoenvironmental Engineering*, *145*(4), 04019008.

Muir Wood, D. (2004). *Geotechnical modelling*. Spon Press, London, UK.

Pestana, J.M. and Whittle, A.J. (1999). Formulation of a unified constitutive model for clays and sands. *International Journal for Numerical and Analytical Methods in Geomechanics*, 23(12), 1215–1243.

Pestana, J. M., Whittle, A. J., & Salvati, L. A. (2002). Evaluation of a constitutive model for clays and sands: Part I–sand behaviour. *International journal for numerical and analytical methods in geomechanics*, *26*(11), 1097-1121.

Pestana, J. M., Whittle, A. J., & Gens, A. (2002). Evaluation of a constitutive model for clays and sands: Part II–clay behaviour. *International journal for numerical and analytical methods in geomechanics*, *26*(11), 1123-1146.

Price, A.B., Boulanger, R.W. and DeJong, J.T. (2019). Centrifuge modeling of variable-rate cone penetration in low-plasticity silts. *Journal of Geotechnical and Geoenvironmental Engineering*, 145(11), 04019098. http://doi.org/10.1061/(ASCE)GT.1943-5606.0002145

Robertson, P.K. (2009). Interpretation of cone penetration tests – a unified approach. *Canadian Geotechnical Journal,* 46(11), 1337-1355.

Sawyer, B.D. (2020). *Cone penetration testing of coarse-grained soils in the centrifuge to examine the effects of soil gradation and centrifuge scaling*. MS thesis, University of California, Davis.

Sturm, A.R. (2019). *On the liquefaction potential of gravelly soils*. PhD thesis, University of California, Davis.

Uesugi, M., and H. Kishida. 1986. "Frictional resistance at yield between dry sand and mild steel." Soils Found. 26 (4), 139–149. https://doi.org/10.3208/sandf1972.26.4_139.